processes

MDPI

Article

Rational Design and CFD Modeling of Innovative Jet Nozzles with a Streamlined Body

Ivan Pavlenko [1], Vadym Baha [2], Marek Ochowiak [3,*], Magdalena Matuszak [3] and Oleh Chekh [2]

[1] Department of Computational Mechanics Named After Volodymyr Martsynkovskyy, Sumy State University, 116, Kharkivska St., 40007 Sumy, Ukraine; i.pavlenko@cm.sumdu.edu.ua
[2] Department of Technical Thermal Physics, Sumy State University, 116, Kharkivska St., 40007 Sumy, Ukraine; v.baga@kttf.sumdu.edu.ua (V.B.); o.cheh@kttf.sumdu.edu.ua (O.C.)
[3] Department of Chemical Engineering and Equipment, Poznan University of Technology, 60-965 Poznan, Poland; magdalena.matuszak@put.poznan.pl
* Correspondence: marek.ochowiak@put.poznan.pl

Abstract

The use of confuser–diffuser nozzles in power machines enables efficient conversion of gas energy into mechanical work. However, traditional Laval, Venturi, and Vitoszynski nozzles are associated with shock wave formation, causing energy losses, noise, and structural loading. This study proposes innovative jet nozzles with an internal streamlined body that forms annular flow rather than a classical diffusor. A rational computational design methodology based on the Venturi effect criterion and equality of cross-sectional area variation laws was developed. A couple of configurations with spindle-toroidal and ellipsoidal streamlined bodies were generated analytically, studied numerically, and confirmed experimentally. Based on the SST turbulence model, CFD simulations for a compressible flow (air) show that the proposed designs reduce the pressure jump from 60 kPa (traditional nozzle) to 20 kPa for the spindle-toroidal configuration and eliminate it for the ellipsoidal configuration. The Reynolds number in the throat decreases by a factor of 2.6, reducing turbulence. The outlet velocity increases by 3.0% for the spindle-toroidal design, while the ellipsoidal nozzle provides expansion with slightly lower velocity but a smoother velocity profile. Experimental thrust measurements agree with simulations within 2.6–6.7%. The proposed designs enhance energy efficiency, reduce erosion and vibration, and enable adaptive flow control via axial displacement of the streamlined body.

Keywords: jet nozzle; streamlined nozzle design; pressure change; velocity distribution; hydraulic efficiency; process innovation

Check for updates

Academic Editor: Iván García Kerdan

Received: 24 February 2026
Revised: 4 April 2026
Accepted: 7 April 2026
Published: 8 April 2026

Copyright: © 2026 by the authors. Licensee MDPI, Basel, Switzerland. This article is an open access article distributed under the terms and conditions of the Creative Commons Attribution (CC BY) license.

1. Introduction

Jet nozzles with variable cross-section channels, including baffle–diffuser ones, are used to accelerate the working fluid (gas, mechanical mixture, fuel, etc.) to the specified hydrodynamic characteristics of power equipment [1,2], as well as environmental technology and innovation [3,4]. They are also widely used in elements of supersonic nozzle devices to direct the gas flow through the turbine, as well as in heat and power plants (heat exchangers, boiler rooms, combustion chambers, etc.), where subsonic modes are used [5,6].

Venturi nozzles were chosen as a traditional design used in systems for transporting and controlling the flow of liquids and gases. These devices are widely used in aviation, energy systems, pneumatics, and the chemical industry, among other applications. In

particular, the Venturi effect is used to mix phases by creating a vacuum at the narrowest cross-section of the nozzle under certain conditions. Since changing the operating parameters shifts the rarefaction zone in the nozzle, any nozzle requires a thorough study for its effective use.

One of the main factors affecting nozzle efficiency is the nozzle's geometric and hydrodynamic characteristics [7]. Since the nozzles have a confuser–diffuser shape, they can operate in supersonic mode. This allows for a significant increase in thrust with only a relatively small increase in the working medium's mass flow rate [8].

Simultaneously, undesirable phenomena arise in off-design and transient regimes, accompanied by specific aerodynamic and thermodynamic characteristics. First, shock waves occur, leading to local, sudden changes in pressure, temperature, and velocity [9]. Secondly, air resistance increases sharply at a critical pressure change (the so-called sound barrier). To overcome this adverse effect, it is necessary to provide additional power and create streamlined aerodynamic shapes to reduce shock waves and energy losses [10].

Equally important is streamlining the profile in the flow, as even minor changes in nozzle geometry can significantly alter pressure and velocity [11]. Flow separation and vortices that arise in supersonic turbulent flow reduce the efficiency of energy conversion and cause additional, including cyclic, loads on structural elements [12].

A variety of recent publications on nozzle design also highlight the significance of the problem under study. In particular, Zocca et al. [13] developed a software tool for the direct design of supersonic nozzle geometry and flow analysis in off-design regimes, free of shock waves. However, the possibility of shock waves occurring when parameters deviated was not considered. Moreover, using external libraries increases computational complexity and complicates integration into engineering packages.

Wu et al. [14] applied an experimental method that allows non-contact investigation of two-phase processes inside opaque nozzles. As a result, it was shown that the inlet-included angle significantly affects the occurrence of cavitation and the development of cavities. However, the limited parameter range limits the applicability of the proposed approach, as it considers only the inlet geometry.

Dai and Haddad [15] used the method of characteristics to synthesize the profile of the supersonic part of the nozzle. As a result, flow parallelism at the outlet, a uniform distribution of parameters, and a given Mach number at the outlet were ensured. The results were compared with CFD simulations realized in ANSYS Fluent v. 2021. However, the idealized assumptions of the model regarding isentropy, the absence of viscosity and turbulence, and the absence of thermal effects limit the CFD verification of the proposed model.

A numerical study of the development of a cavitation pocket in a Venturi nozzle was performed by Charrière et al. [16]. Based on a new semi-empirical dependence with a free parameter, a non-stationary dynamic problem of heat and mass transfer in a nozzle is considered. However, despite comparisons with other models, the presence of a free parameter limits the approach's versatility and requires additional calibration.

De la Cruz-Ávila et al. [17] investigated cavitation phenomena in a Venturi nozzle based on considering the non-stationary development of a vapor cloud. The use of non-stationary Reynolds equations allowed us to obtain the flow structure and pressure distribution. However, the rectangular cross-section geometry and the dependence of the results on the turbulence model limit the consideration of hydrodynamic regimes and lead to incompleteness in the interfacial interaction model.

Two-phase gas–liquid jets with increased impact force were studied by Shi et al. [18]. The use of the volume-of-fluid approach to describe two-phase flow and the optimization of nozzle geometry enabled investigation of the jet's hydrodynamic characteristics and shock

wave formation. As a result, it was found that the aero-shaped nozzle gives higher pressure than the traditional conical nozzle. Also, a parametric study of geometric factors increased the engineering significance of the proposed approach for hydroabrasive machining, surface cleaning, drilling, and medical jet technologies. However, the lack of an optimization algorithm, experimental validation, and a relatively narrow range of modes limit the reliability of the obtained results.

Atmaca et al. [19] studied free jets for different types of nozzles (circular, rectangular, 2D-contour). This allows us to compare the influence of nozzle geometry on jet development. Also, a parametric analysis was performed for different flow conditions. As a result, the jet's axial velocity was measured at various distances from the nozzle exit. However, nozzles with a variable profile were not considered. The range of Reynolds numbers and the effects of temperature are not specified. The limited experimental base (a dataset from the literature was used) makes it difficult to generalize the results.

Tip ring and elliptic supersonic nozzles were studied by Rao and Jagadeesh [20] to intensify mixing in supersonic jets, which is critical for ejectors. The use of laser imaging in the study of 3D jet structures is an essential experimental contribution. As a result, it was shown that, when used in a supersonic ejector, both nozzles provide greater entrainment of the secondary flow, thereby improving ejector efficiency. However, the study was limited by a single Mach number and by geometry optimization. Also, the intensification of mixing in supersonic jets can cause acoustic waves and resonance phenomena. However, these aspects were not investigated.

West [21] realized a comprehensive experimental and numerical study of the cavitation jet formed by a nozzle with a triangular hole. As a result, the power dependence of the length of the steam jet on the volume fraction of steam was established. This enabled us to derive new empirical equations and develop a predictive model to determine the jet's effective length. However, the limited nozzle geometry and the narrow range of hydrodynamic modes (Reynolds numbers) limit the applicability of the results and their interpretation to real-world applications.

Research on hydrodynamics and heat and mass transfer of a jet formed in a combined annular-conical nozzle was conducted by Shuja et al. [22]. As a result, it was shown that such nozzles increase convective heat and mass transfer in confined geometries, which has practical significance for thermal control systems and the cooling of high-temperature elements, as well as for improving the energy efficiency of industrial processes. However, the lack of experimental validation of the outlet jet velocity limits the reliability of the results obtained. Also, non-stationary phenomena, pulsations, and transient regimes were not considered.

Narimani et al. [23] proposed a combined approach to nozzle geometry optimization using a genetic algorithm. This allowed the center of the body to be represented as a Bezier curve, providing a smooth change in shape and the ability to control the exit angle of the flow. However, the results obtained are limited to a single nozzle with a conical streamline. The influence of turbulence and flow fluctuations on the optimization was also not accounted for.

A new type of annular nozzle for particle flow control was proposed by Rukosuyev et al. [24]. It was stated that the use of an ultrasonic atomizer provides controlled droplet dispersion, which affects particle size, and allows the atomization frequency to be adjusted in response to different process parameters. However, the study was limited to a single nozzle geometry and a limited number of influencing parameters (the effects of gas flow rate and pressure distribution were not evaluated).

Wang et al. [25] realized a comprehensive numerical study of annular nozzles of various configurations. As a result, the relationship between geometry and jet characteristics

is established, as is how individual elements (channel width and curvature) affect the gas flow, shock waves, and total pressure losses. However, the lack of experimental validation limits the numerical results. Also, due to CFD simulations, there may be errors in the modeling of turbulence and shock waves.

A practical study on the application of jet impact on a flat surface in surface treatment was realized by Shuja [26]. A comparison of different nozzle types (conical and annular) showed how nozzle geometry affects the flow structure, heat transfer, and contact interaction with the treated surface. However, since the results are entirely numerical, without experimental confirmation of specific cone angles or nozzles, this limits reliability and the scope of application.

The main scientific contributions, advantages, and limitations of the above-mentioned studies are summarized in Table 1.

Table 1. A comparative analysis of the scientific background.

Reference	Scientific Contribution	Advantages	Drawbacks and Limitations
Supersonic nozzles			
Zocca et al. [13], 2023	Developed software for direct design of supersonic nozzle geometry and flow analysis in off-design regimes without shock waves	Allows direct nozzle design; analysis of off-design conditions	Shock wave occurrence was not considered; use of external libraries increases computational complexity and complicates integration
Charrière et al. [16], 2015	Numerical study of cavitation pocket development in a Venturi nozzle with a semi-empirical relation	Considers unsteady heat and mass transfer dynamics	Free parameter limits versatility and requires calibration
De la Cruz-Ávila et al. [17], 2024	Investigated cavitation in a Venturi nozzle using unsteady Reynolds equations	Determined flow structure and pressure distribution	Rectangular cross-section and turbulence model dependence limit hydrodynamic regime modeling
Shi et al. [18], 2025	Studied two-phase gas–liquid jets and optimized nozzle geometry	Aero-shaped nozzle gives higher pressure; parametric study useful for hydroabrasive machining, cleaning, drilling, and medical jets	No optimization algorithm, experimental validation, or wide range of operating modes
Rao and Jagadeesh [20], 2014	Studied tip ring and elliptic supersonic nozzles for enhanced mixing in supersonic jets	Laser imaging of 3D jet structure; improved entrainment and ejector efficiency	Single Mach number; geometry not optimized; acoustic effects not investigated
West [21], 2025	Experimental and numerical study of cavitation jet through a triangular-hole nozzle	Established steam jet length vs. steam fraction; developed predictive model	Limited nozzle geometry; narrow range of Reynolds numbers
Shuja et al. [22], 2009	Studied hydrodynamics, as well as heat and mass transfer in a combined annular-conical nozzle	Enhanced convective heat and mass transfer; practical significance for thermal control and energy efficiency	No experimental validation of outlet velocity; unsteady phenomena, pulsations, and transient regimes were not considered
Narimani et al. [23], 2024	Nozzle geometry optimization using a genetic algorithm with Bezier curve representation	Smooth shape variation; control of exit flow angle	Results limited to a single conical streamline nozzle; turbulence and flow fluctuations not accounted for

Table 1. *Cont.*

Reference	Scientific Contribution	Advantages	Drawbacks and Limitations
Shuja [26], 2005	Practical study of jet impingement on a flat surface with different nozzle types	Showed the effect of nozzle geometry on flow, heat transfer, and contact with the surface	Entirely numerical results; no experimental validation of specific cone angles or nozzles
Supersonic and subsonic nozzles			
Dai and Haddad [15], 2024	Synthesized a supersonic nozzle profile using the method of characteristics	Ensures outlet flow parallelism, uniform parameter distribution, and specified Mach number	Idealized assumptions (isentropic, no viscosity or turbulence, no thermal effects) limit CFD validation
Atmaca et al. [19], 2021	Studying free jets from various nozzle types; compared geometry effects	Parametric analysis performed; axial velocity measured at different distances	Variable profile nozzles not considered; limited experimental dataset; Reynolds number and temperature effects not specified
Wang et al. [25], 2025	Comprehensive numerical study of annular nozzles of various configurations	Established relationship between geometry and jet characteristics, shock waves, and pressure losses	No experimental validation; CFD may introduce errors in turbulence and shock-wave modeling
Other nozzles			
Wu et al. [14], 2024	Experimental method for non-contact investigation of two-phase processes inside opaque nozzles	Showed the effect of inlet angle on cavitation; access to internal processes	Limited parameter range: only the inlet geometry is considered
Rukosuyev et al. [24], 2018	Proposed new annular nozzle for particle flow control with ultrasonic atomizer	Controlled droplet dispersion; adjustable atomization frequency	Only one nozzle geometry studied; limited number of influencing parameters (gas flow rate, pressure distribution not evaluated)

The proposed article aims to increase the efficiency of confuser–diffuser nozzles by developing rational designs with an internal streamlined body that generates an annular compressible flow and suppresses local pressure change.

The work suggests replacing traditional nozzles with innovative self-regulating designs with an internal streamlined body—an insertable element of variable cross-section with the possibility of further axial movement. In this case, instead of the constricting–expanding shape of the outer wall, an annular gas flow forms around the streamlined body.

The advantage of the proposed solution is the ability to further control the nozzle's operating characteristics by adjusting the position of the streamlined body, thereby creating design features that allow rotation around the axis of symmetry. All these open opportunities to rationally influence the flow structure, pressure, and velocity field distributions along the nozzle length, thereby increasing energy efficiency, adapting the nozzle to the installation, and expanding the scope of application.

The scientific novelty of the work lies in the development, theoretical substantiation, and validation of a fundamentally new concept of jet nozzles with a rationally designed, internally streamlined body that transforms a conventional confuser–diffuser flow into a controlled annular compressible flow, thereby suppressing local pressure change and smoothing flow velocity profile.

The article's structure is as follows. Section 2 describes the research methodology. First, Section 2.1 describes the traditional model with tabular data on geometric parameters and their changes. The main characteristics regarding thermodynamic calculation are also

given. After that, the research methodology and the primary settings of CFD simulations are described in Section 2.2. In the final Section 2.3, an experimental setup is presented. A brief description of the measuring technique is also provided.

An innovative approach to the rational design of jet nozzles is presented in Section 3.1 in a general analytical form. The effectiveness of the proposed approach in terms of hydraulic characteristics is justified in Section 3.2. Section 3.3 describes the numerical results for the traditional model. The obtained results are substantiated by thermodynamic calculations and by comparison with the experimental data given in Section 3.4.

After that, rational designs of innovative jet nozzles are presented in Section 3.5. In particular, the spindle-toroidal-shaped streamlined body is described in Section 3.5.1, and the ellipsoidal-shaped streamlined body is described in Section 3.5.2. The obtained analytical results are supported by the corresponding CFD calculations for the above-mentioned innovative designs (Section 3.6, with Sections 3.6.1 and 3.6.2 for each of the two proposed designs).

Analytical calculations and numerical simulations are accompanied by an analysis of the results, in particular their main advantages and limitations. Based on the comparative study of the designs, a prototype of an innovative nozzle is proposed in Section 3.7 with a corresponding assembly drawing. Finally, a comparative table of expected characteristics is discussed.

The primary achievements and their significance are stated in the conclusions. Ways for further research are also formulated. After the conclusions, the program code of the developed methodology to automatically obtain the nozzle geometry is given in Appendix A.

2. Materials and Methods

2.1. A Model Description

Figure 1 illustrates the internal profile of an axisymmetric Venturi nozzle, designed as a body of revolution with a circular cross-section.

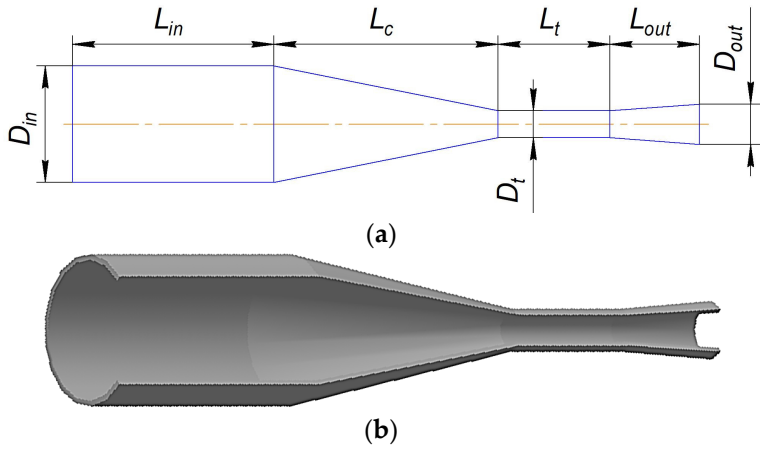

Figure 1. The design scheme of the Venturi nozzle: (**a**) design scheme; (**b**) cross-sectional view.

The total axial length of the device

$$L = L_{in} + L_c + L_t + L_{out} \quad (1)$$

is divided into four distinct functional sections with the following lengths (Table 2): L_{in}—length of the inlet cylinder with inlet diameter D_0, m; L_c—length of the conical-shaped confuser with outlet diameter D_t, m; L_t—length of the cylindrical throat, m; and L_{out}—length of the conical-shaped diffusor with the outlet diameter D_{out}, m.

Table 2. Design features of the Venturi nozzle.

Section	Part Name	Length, m	Diameter, mm	
			Inlet	Outlet
Section 1	Cylindrical inlet	L_{in} = 0.045	D_0 = 0.026	
Section 2	Conical-shaped confuser	L_c = 0.050	D_0 = 0.026	D_t = 0.006
Section 3	Cylindrical throat	L_t = 0.025	D_t = 0.006	
Section 4	Conical-shaped diffuser outlet	L_{out} = 0.020 *	D_t = 0.006	D_{out} = 0.009

* It can range between 0.020, 0.080, 0.160, and 0.300 m.

The initial part consists of a cylindrical inlet with a constant diameter D_0 = 0.026 m and a length L_{in} = 0.045. This part is designed to smooth the velocity profile of the working medium before narrowing. This also minimizes errors in subsequent CFD calculations by ensuring a fully developed velocity profile before the fluid enters the compression zone.

The second part is a conical-shaped confuser with a length L_c = 0.050 m. It features a significant reduction in diameter from inlet D_0 = 0.026 m to throttle D_t = 0.006 m. The relatively high inlet-to-throat diameter ratio ($\beta_{in} = D_t/D_0 = 0.23$) facilitates rapid conversion of static pressure into kinetic energy, thereby accelerating the flow.

The third part is a cylindrical throat with a length *of* L_t = 0.025 m and a narrowest diameter of D_t = 0.006 m. The extended length-to-diameter ratio of the throat ($L_t/D_t = 4.2 >> 1$) helps stabilize the flow, which is critical for suction performance in ejector systems.

The final part of a nozzle is a conical diffusor with a length L_{out} = 0.020–0.300 m, where the diameter increases from D_t = 0.006 m to D_{out} = 0.009 m (a throat-to-outlet diameter ratio $\beta_{out} = D_{out}/D_t = 1.50$). This section is designed for pressure stabilization and controlled acceleration of the fluid flow.

The outlet half-angle

$$\theta = atan\left(\frac{D_{out} - d_t}{2L_{out}}\right) \quad (2)$$

ranges from 0°17′ to 4°29′ depending on the outlet lengths L_{out}.

The relatively short lengths L_{out} = 0.020–0.080 m suggest a design priority for jet formation ($tan(\theta)$ from 1:1.9 to 1:3.5) rather than total pressure restoration for L_{out} = 0.160–0.300 m (θ from 4°29′ to 1°44′).

Nozzle asymmetry (i.e., the convergent section does not equal the divergent section) is typical of specialized jet devices (e.g., ejectors, flowmeters, jet pumps) where precise flow acceleration is more critical than downstream pressure recovery efficiency.

The initial analytical calculations of the pressure ratio, outlet velocity, and Mach number are critical to understanding how the gas will behave inside the nozzle. Since the nozzle has a significant diameter reduction (from D_{in} = 0.026 m to D_t = 0.006 m), it can significantly accelerate the flow, leading to specific aerodynamic phenomena.

The theoretical outlet velocity for an ideal isentropic expansion can be evaluated from the energy equation as follows:

$$v_{out}^* = \sqrt{\frac{2\gamma}{\gamma - 1} RT_0\left(1 - \psi^{\frac{\gamma}{1-\gamma}}\right)}, \quad (3)$$

where γ—heat capacity ratio; R = 287 J/(kg·K)—the ideal gas constant; T_0 = 300 K—an opening temperature (corresponds to 23 °C); ψ—pressure ratio.

Considering air treated as an ideal gas with heat capacity ratio γ = 1.4, for the inlet-to-outlet pressure ratio $\psi = p_{in}/p_{out} = 6$ ($p_{in} = 6 \times 10^5$ Pa—inlet pressure, and $p_{out} = 1 \times 10^5$ Pa—outlet pressure), the resulting theoretical velocity v_{out}^* = 491 m/s is therefore in the sonic range.

However, because of the compressible nozzle flow, this value could be much higher, in the supersonic range. For a more precise evaluation, special attention should be paid to possible regions of local pressure change in supersonic flow. The critical pressure ratio for choked flow in a converging section is as follows [27]:

$$\frac{p_{cr}}{p_{in}} = \left(\frac{2}{\gamma+1}\right)^{\frac{\gamma}{\gamma-1}} \approx 0.528, \quad (4)$$

where p_{cr}—critical pressure, Pa.

According to Equation (4), the critical pressure at the throat $p_{cr} = 0.528 \times 6 \times 10^5 = 3.17 \times 10^5$ (Pa).

Since the outlet static pressure $p_{out} = 1 \times 10^5$ Pa is significantly lower than the critical pressure, the flow is expected to change at the throat (Mach number $M = 1$). Therefore, the flow accelerates from subsonic at the inlet to sonic at the throat, and supersonic in the diverging section. The throttling effect limits the mass flow rate and becomes independent of further reductions in downstream pressure. Therefore, shock waves are expected in the initial model.

The Mach number can also be estimated from the isentropic relation:

$$\frac{p_{in}}{p} = \left(1 + \frac{\gamma-1}{2}M^2\right)^{\frac{\gamma}{\gamma-1}}, \quad (5)$$

where p—pressure, Pa.

Particularly, the outlet Mach number is as follows:

$$M_{out} = \sqrt{\frac{2}{\gamma-1}\left(\psi^{\frac{\gamma}{\gamma-1}} - 1\right)}, \quad (6)$$

where $\psi = p_{in}/p$—pressure ratio.

According to Equation (6), for the inlet-to-outlet pressure ratio $\psi = 6$, the outlet Mach number $M_{out} = 1.8$. The corresponding outlet velocity v_{out} is therefore in the supersonic range. Further, this will provide a reliable baseline for validating subsequent CFD simulation results and interpreting deviations caused by viscous, turbulent, and geometric effects.

2.2. CFD Modeling Parameters and Settings

The flow through the nozzle was simulated using a steady-state computational fluid dynamics (CFD) model implemented in ANSYS CFX 2025 R2. According to the previous authors' experience in modeling nozzles [28,29], the following parameters were chosen. The working fluid was air, modeled as an ideal gas with variable density, which is appropriate for compressible flow with a pressure ratio of 6:1. The flow was assumed to be turbulent, compressible, and single-phase.

The computational domain was discretized using a structured-dominant mesh consisting of about 4.0×10^5 elements. The mesh was primarily composed of hexahedral elements, supplemented by a relatively small number of wedge elements (less than 0.5%). No tetrahedral, pyramidal, or polyhedral elements were used. This is advantageous for resolving boundary layers and minimizing numerical diffusion.

The mesh quality metrics indicate adequate numerical resolution and element quality. The minimum face angle was 41°42′, while the maximum face angle was 132°12′. The maximum edge length ratio was 9.8, and the maximum element volume ratio was 10.5. The connectivity range of 2–10 was within acceptable limits, indicating a well-formed grid suitable for engineering-level accuracy.

A mesh independence study was performed using three progressively refined meshes (Table 3).

Table 3. The grid convergence study results.

Number of Elements	Number of Inflation Layers	Dimensionless Wall Distance y^+ Inlet	Outlet
1.9×10^5	2	2.6	5.2
2.2×10^5	4	2.2	4.2
2.9×10^5	8	2.1	4.2
4.0×10^5	16	2.1	3.2

A dimensionless wall distance y^+ as a key parameter shows the grid convergence for 16 inflation layers (4.0×10^5 elements), confirming mesh-independent results. The final mesh is presented in Figure 2.

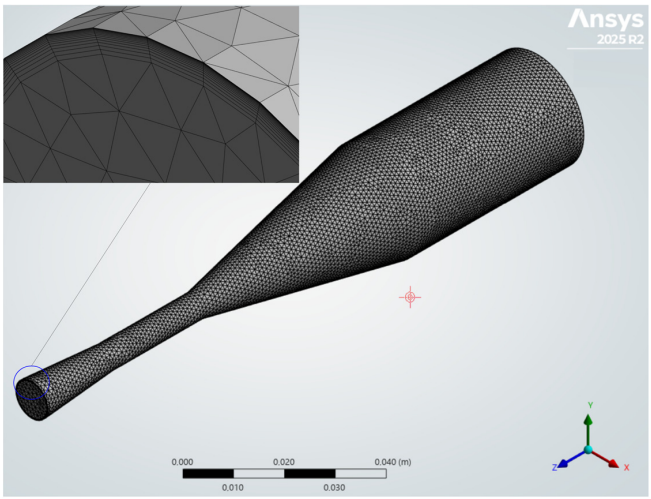

Figure 2. The final mesh.

The simulations were performed in a stationary fluid domain. Buoyancy effects were neglected because forced convection and pressure-driven flow were dominant over gravitational effects. Heat transfer was modeled using the total energy formulation, including viscous work effects. This formulation is physically consistent for high-speed internal flows, where compressibility effects are significant.

Turbulence was modeled using the shear stress transport (SST) model, which combines the advantages of the k–ω model near the wall and the k–ε model in the free stream. Based on previously reported simulation data for conventional nozzle configurations using k–ε and standard k–ω turbulence models [30], it has been demonstrated that the SST model provides more consistent predictions in regions with adverse pressure changes. Moreover, the discrepancies between the models remain within acceptable limits, thereby supporting the robustness and suitability of the selected approach [31].

Automatic wall treatment was applied, allowing appropriate resolution of the near-wall region depending on the local mesh density. This formulation is suitable for nozzle-type flows, providing accurate near-wall predictions while maintaining robustness in the core. Moreover, the automatic wall-function approach is acceptable for engineering simulations, provided the near-wall mesh resolution falls within the expected y^+ range. The dimensionless wall distance y^+ in a range of 2.1 (for the inlet) and 3.2 (for the outlet) is suitable for the SST model, ensuring proper resolution of the boundary layer.

The boundary conditions were specified as follows. A subsonic inlet was chosen with flow direction normally to the boundary. The total pressure was set to 6×10^5 Pa, and the static temperature was specified as T_0 = 300 K (23 °C). Medium turbulence intensity, with an eddy viscosity ratio defined as the ratio of turbulent to molecular viscosity, was assumed, serving as a key metric for quantifying turbulence strength relative to molecular diffusion. Such a choice is commonly used in CFD modeling to specify inlet boundary conditions and assess boundary-layer resolution. An opening boundary condition with a relative static pressure of 1×10^5 Pa and the opening temperature T_0 = 300 K (23 °C) was chosen as an outlet. Medium turbulence intensity was also prescribed. All solid boundaries were modeled as no-slip adiabatic smooth surface walls.

The governing equations for mass, momentum, and energy conservation were solved in ANSYS CFX using a finite volume method. The compressible formulation accounted for density variations according to the ideal gas law. The steady-state solution was obtained using the default high-resolution advection scheme available in ANSYS CFX.

The above formulation provides a physically consistent representation of compressible turbulent flow through a nozzle at a pressure ratio of 6:1 and enables detailed analysis of velocity, pressure, and Mach number distributions within the flow domain.

2.3. Experimental Setup

To additionally prove the reliability of the CFD modeling, experimental studies of the nozzle design were also conducted. For this purpose, a weight method was used to measure the jet's reactive force. The corresponding stand and principal scheme according to the international standards ISO 1219-1:2012 [32] and ISO 14617-1:2025 [33] are presented in Figure 3.

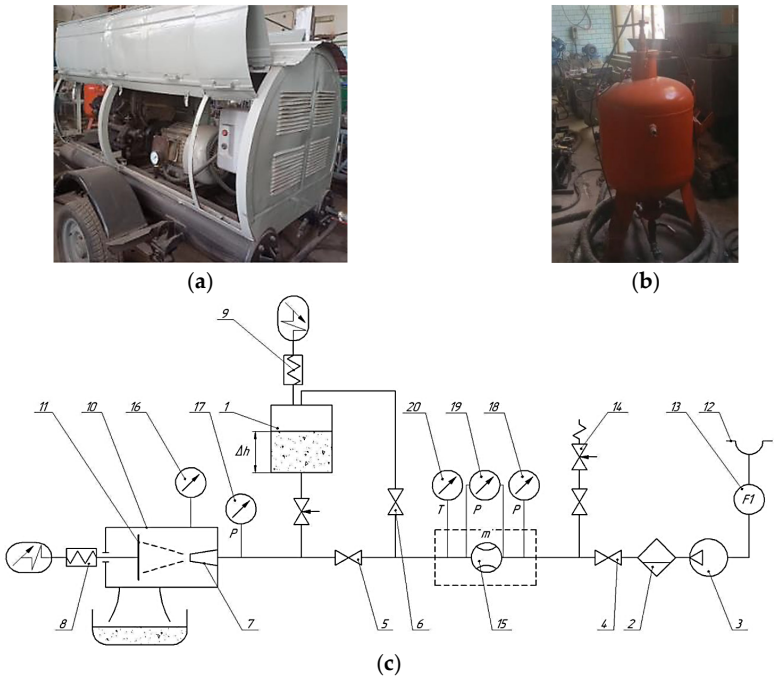

Figure 3. Compressor station PKS-5.25 (**a**), jet apparatus (**b**), and principal scheme of the stand (**c**): 1—container with a working medium; 2—dehumidifier; 3—compressor; 4–6—shut-off valves; 7—nozzle; 8—dynamometer, 9—dynamometer, 10—jet reaction measuring device; 11—plate under loading; 12—air intake; 13—air flow meter; 14—safety valve; 15—flowmeter washer; 16, 17–19—pressure gauges; 20—thermometer.

The working medium enters container 1, suspended on a crane beam, via a crane scale OCS-0.5-X2L (Axis®, Lviv, Ukraine) with medium accuracy class, in accordance with EN

45501:2015 [34]. Air is used as the carrier flow, which, after passing through the compressor 3, enters the nozzle 7 after the air intake 12, the moisture separator 2, and the shut-off valves 4–6. Nozzle 7 accelerates the flow to the required speed for the installation to work. The working flow hits the loading plate 11, which is connected to dynamometer 8. In this way, the load force on plate 11 is measured.

The stand is also equipped with a flow-measuring washer 15, which is used to set the air flow rate through the nozzle 7 by measuring the pressure drop on the pressure gauges 18, 19. Hydraulic losses in the installation are determined from the pressure difference between gauges 16 and 17. The flow temperature is controlled using thermometer 20. The safety valve 14 prevents the pressure from exceeding the critical value.

3. Results

3.1. An Innovative Approach for the Rational Design of Jet Nozzles

Despite traditional Venturi nozzles, which in power machines enable more efficient conversion of gas energy into mechanical work, they create local pressure change and thermal and aerodynamic loads that should be accounted for in the design. To overcome this challenge, it is proposed to replace traditional nozzles with innovative self-regulating designs with an internal streamlined body—an insertable element of variable cross-section (Figure 4a).

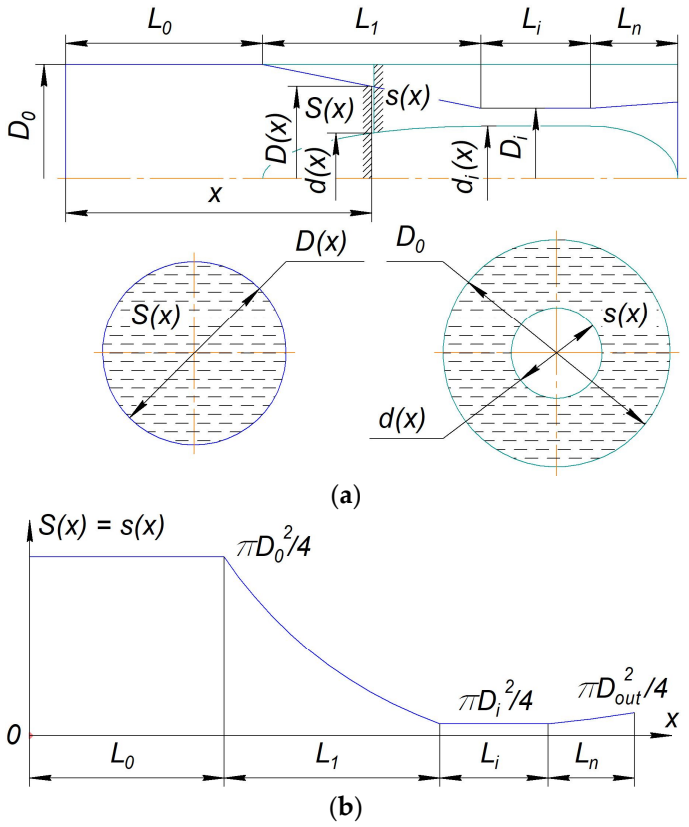

Figure 4. The design schemes (**a**) of nozzles (blue line—the initial design; green line—the design with a streamlined body and cylindrical wall) and change in the cross-sectional areas (**b**).

Figure 4 contains the following designations: x—longitudinal coordinate, m; D_0, L_0—inlet diameter and length, respectively; $D(x)$—cross-sectional diameter of the traditional nozzle at the coordinate x; D_i—cross-sectional diameter of the i-th section of the nozzle; $d_i(x)$—unknown function of change in cross-sectional diameter for the streamlined body, corresponding to the i-th part of the initial nozzle; $d(x)$—unknown overall function of

change in the cross-sectional diameter for the streamlined body; L_n—length of the outlet part for the traditional nozzle (n—the total number of different cylindrical-shaped and conical-shaped parts); and $S(x)$, $s(x)$—cross-sectional areas of the flow at the coordinate x for the traditional and new nozzles, respectively.

The shape of the streamlined body should be rationally justified in terms of compliance with the Venturi effect. Therefore, the following generalized approach to their design is proposed. First, the inlet diameter D_0 is chosen as a reference. As a basic concept, it is suggested to assume equality of the laws of change along the length for the cross-sectional areas of the new annular and basic cylindrical channels. (Figure 4b):

$$s(x) = S(x). \tag{7}$$

After considering the geometrical dependencies

$$S(x) = \frac{\pi D^2(x)}{4};\ s(x) = \frac{\pi D_0^2}{4} - \frac{\pi d^2(x)}{4}, \tag{8}$$

the following expression can be obtained for the law of change in the diameter of the streamlined body:

$$d(x) = \sqrt{D_0^2 - D^2(x)}. \tag{9}$$

Therefore, to obtain an analytical dependence for the diameter $d(x)$, the reliance for the piecewise continuous function $D(x)$ should be presented analytically. For this purpose, the following expression is used for the i-th section (Figure 4a):

$$D_i(x) = D_{i-1} + \frac{D_i - D_{i-1}}{L_i}\left(x - \sum_{k=0}^{i-1} L_k\right);\ i \geq 1;\ \sum_{k=0}^{i-1} L_k \leq x < \sum_{k=0}^{i} L_k, \tag{10}$$

where k—index of summation.

Therefore, a change in the diameter of the streamlined body (9) is as follows:

$$d_i(x) = \sqrt{D_0^2 - \left[D_{i-1} + \frac{D_i - D_{i-1}}{L_i}\left(x - \sum_{k=0}^{i-1} L_k\right)\right]^2}, \tag{11}$$

To combine all the piecewise continuous functions $d_i(x)$ into an overall function over all n parts, the following summation is applied:

$$d(x) = \sum_{i=0}^{n} d_i(x) H\left(x - \sum_{k=0}^{i-1} L_k\right)\left[1 - H\left(x - \sum_{k=0}^{i} L_k\right)\right], \tag{12}$$

where $H(\cdot)$—the Heaviside function, applied to truncate elements on the left and right sides of the i-th part.

Two different options for applying the developed method are considered in Sections 3.5.1 and 3.5.2.

3.2. An Efficiency of the Proposed Designs

In the proposed designs, turbulence in the throat region is reduced by decreasing the Reynolds number. Particularly, for the traditional design with cylindrical flow, for which the hydraulic diameter equals the throat diameter D_t, the Reynolds number is determined by the following dependency:

$$Re_c = \frac{\rho v_t D_t}{\mu}, \tag{13}$$

where μ—dynamic viscosity of the air, Pa·s.

However, for the developed designs with annular flows, the hydraulic diameter of the annular channel is as follows:

$$D_h = \frac{4S_a}{\Pi_a}, \tag{14}$$

where S_a—the cross-sectional area in the throat part, m^2; Π_a—the perimeter of the cross-sectional contour, m.

The maximum diameter of the streamlined body is as follows:

$$d_{max} = \sqrt{D_{out}^2 - D_t^2}. \tag{15}$$

It can be shown that $S_a = S_t$. This is due to the initial Equation (7) with the dependencies (8), (9) and (15).

$$S_a = \frac{\pi D_{out}^2}{4} - \frac{\pi d_{max}^2}{4} = \frac{\pi D_t^2}{4} = S_t, \tag{16}$$

Also, considering Formula (15), the perimeter of the annular channel is as follows:

$$\Pi_a = \pi D_{out} + \pi d_{max} = \pi(D_{out} + d_{max}) = \pi\left(D_{out} + \sqrt{D_{out}^2 - D_t^2}\right). \tag{17}$$

Considering Formulas (16) and (17), the hydraulic diameter (14) takes the following form:

$$D_h = \frac{D_t^2}{D_{out} + \sqrt{D_{out}^2 - D_t^2}} = \frac{D_t}{\psi + \sqrt{\psi^2 - 1}}, \tag{18}$$

Therefore, the Reynolds number for the proposed annular channels is reduced:

$$Re_a = \frac{\rho v_t D_h}{\mu} = \frac{Re_t}{K}; \;\; K = \psi + \sqrt{\psi^2 - 1} \tag{19}$$

where K—the turbulence reduction factor.

Such an effect provides several essential engineering advantages as follows. First, turbulence is accompanied by additional energy losses due to vortex structures and intense mixing. However, according to Equation (19), the Reynolds number is reduced by K times for the proposed design. This leads to a decrease in friction and, consequently, an increase in the nozzle's total energy efficiency. The erosion of the inner surface of the nozzle also decreases, thereby increasing its service life.

Second, turbulence reduction also reduces local pressure drop. As a result, the risk of flow separation at the nozzle exit is diminished. Moreover, turbulence can reduce acoustic effects and, accordingly, noise and vibrations. However, additional studies are needed.

3.3. Numerical Results for the Traditional Model

The validity of the applied CFD modeling approach is demonstrated for the traditional model by the primary qualitative and quantitative features of pressure, velocity, and temperature distributions along the nozzle length.

Particularly, the axial pressure distribution (Figure 5) exhibits a monotonic decrease from the inlet stagnation region (inlet pressure p_{in} = 600 kPa) toward the nozzle exit (static outlet pressure p_{out} = 60–80 kPa), which is consistent with compressible flow acceleration in a confuser–diffuser nozzle. The velocity increases along with the flow direction, with a gradual acceleration in the converging section and a rapid rise near the throat (Figure 6).

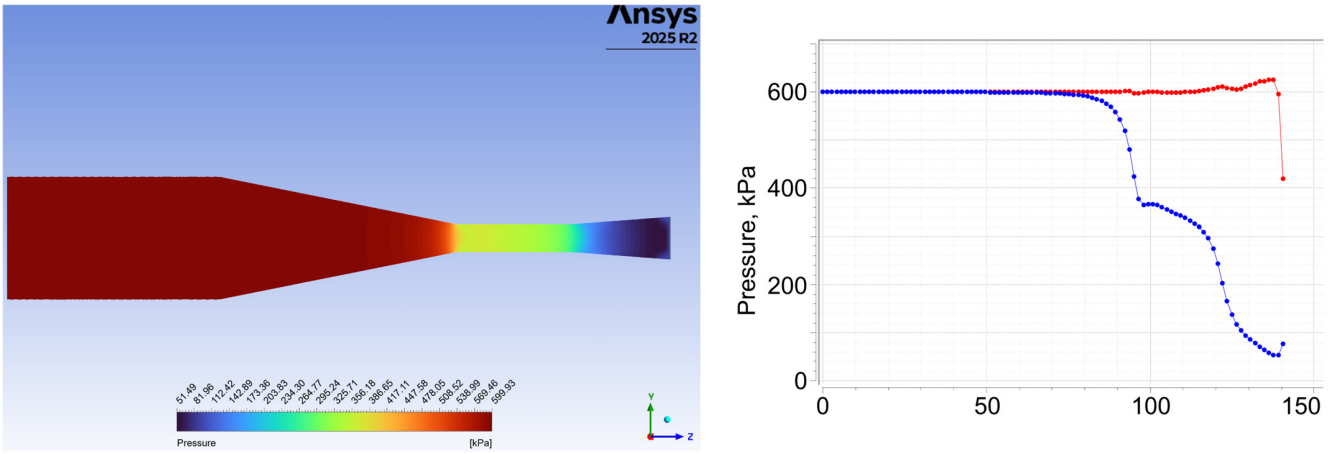

(**a**) (**b**)

Figure 5. Pressure distribution for the traditional nozzle: (**a**) contour plot; (**b**) graphs (red line—total pressure; blue line—static pressure).

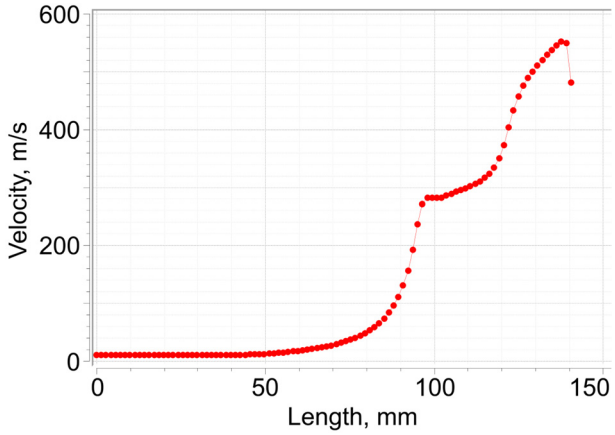

Figure 6. Velocity distribution graph for the traditional nozzle.

At the throat location, the velocity reaches approximately near-sonic speed, as predicted by Equation (3). Also, a local pressure change is available in the vicinity of the throat, where the flow reaches sonic conditions. A pressure change exists because the pressure profile has a local abrupt increase (about 60 kPa) followed by a gradual decrease toward the outlet. Downstream, a gradient change in the velocity also occurs.

Downstream of the throat, the pressure continues to decrease in the diffusor, indicating supersonic expansion. As a result, the velocity continues to increase, indicating supersonic acceleration, as expected. The maximum velocity of about v_{max} = 565 m/s is achieved near the outlet section of the nozzle, which validates the obtained CFD results compared to Equation (5) with the following relative error:

$$\varepsilon_v = \left| \frac{v_{max}}{v^*_{out}} - 1 \right| \cdot 100\%, \tag{20}$$

which does not exceed ε_v = 5.8%.

The static temperature decreases with increasing nozzle length (Figure 7) due to the conversion of internal energy into kinetic energy.

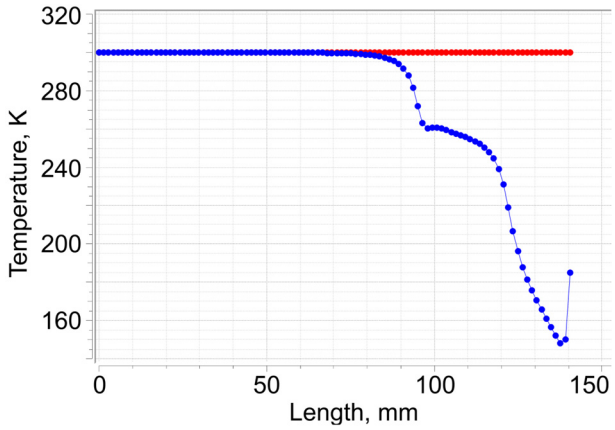

Figure 7. Temperature distribution graphs for the traditional nozzle (red line—total temperature; blue line—static temperature).

The temperature change is most significant in the region where the flow accelerates to sonic and supersonic speeds. A sudden temperature rise additionally indicates a local compression process. Nevertheless, given the adiabatic wall condition, the total temperature (which the gas has while decelerating adiabatically) remains constant (T_0 = 300 K) throughout the flow domain, which is consistent with compressible flow theory [35]:

$$T_0 = T + Pr^n \cdot \frac{v^2}{2c_p}, \tag{21}$$

where T_0—total pressure, K; T—static pressure, K; v—flow velocity, m/s; c_p—heat capacity at constant pressure, J/(kg·K); $Pr = c_p\mu/k_T$—Prandtl number (about 1 for gases); k_T—thermal conductivity, W/(m·K); and n—power (n = 1 for laminar flow, and $n = \frac{1}{3}$ for turbulent flow).

Considering the dynamic viscosity $\mu = 1.82 \times 10^{-5}$ Pa·s, the Reynolds number $Re = 6.9 \times 10^4$, and therefore, $n = \frac{1}{3}$. Also, considering thermal conductivity k_T = 0.026 W/(m·K), the Prandtl number Pr = 0.71. Then, according to Equation (21), after considering heat capacity $c_p = 1.01 \times 10^3$ J/(kg·K), the total temperature for the outlet (static temperature T_{out} = 145 K, and velocity v_{out} = 565 m/s) equals T_{out} = 286 K. This value corresponds to the total temperature T_0 = 300 K with a relative error:

$$\varepsilon_T = \left| \frac{T_{out}}{T_0} - 1 \right| \cdot 100\%, \tag{22}$$

which does not exceed ε_T = 4.7%.

Therefore, the minor relative errors (20) and (22) quantitatively confirm CFD results.

3.4. Validation of the CFD Model by Experimental Results

Air was chosen as the medium for the experiment. The experimental setup allows for research on variable working pressures in the nozzle and for changing the nozzles under study across a wide range of geometric parameters. The controlled parameters are pressure and air flow. During the test, the compressor supplied air into the receiver with a total volume of 1.5 m^3. After reaching a pressure of 0.8 MPa in the receiver, air is supplied to the unit inlet at a given pressure. Ranges of operating parameters of the setup are as follows: air pressure at the inlet to the device: 0.2–0.8 MPa; air pressure at the outlet: 0.1–0.6 MPa; inlet air temperature: 283–303 K; air flow rate: rate does not exceed 0.1 m^3/s.

To achieve a relative error of 5–10% with a confidence probability of 0.90–0.95, at least five measurements of the controlled parameters were performed. The determination of the

values within direct measurement errors was carried out according to the passport data of the measuring tools presented in Table 4.

Table 4. Instrumentation and measuring errors.

Parameter	Measuring Device	Error
Pressure	Manometer MO 0–1 MPa (Alfaprylad Ltd., Kyiv, Ukraine)	±0.5%
Temperature	Digital sensor 220–400 K (Maxim Integrated, San Jose, CA, USA)	±0.2 K
Diameter	Digital caliper (Microtech, Kharkiv, Ukraine)	0.05 mm
Force	Dynamometer AWM-100 (Protester, Kyiv, Ukraine)	±2%

The following aerodynamic dependence determines the jet force:

$$F = C_x \frac{\rho v_{out}^2}{2} S_{out}, \tag{23}$$

where F—pressure force, N; ρ—gas density, kg/m^3; S_{out}—outlet cross-sectional area, m^2; and C_x—drag force coefficient.

Considering the cross-sectional area $S_{out} = \frac{\pi D_{out}^2}{4}$, as well as the thermodynamic dependence for dry air density $\rho = \frac{p}{RT_0}$, the outlet velocity can be evaluated as follows:

$$v_{out} = \frac{1}{D_{out}} \sqrt{\frac{8RT_0F}{\pi C_x p}}, \tag{24}$$

According to common engineering practice, the drag force coefficient is in the range C_x = 1.1–1.2 [36]. An uncertainty of indirect evaluation of the velocity v_{out} was carried out using a Kline and McClintock approach [37], applied to Equation (24):

$$\varepsilon_v = \sqrt{\frac{1}{4}\left(\varepsilon_p^2 + \varepsilon_T^2 + \varepsilon_F^2\right) + \varepsilon_D^2 + \left(\frac{C_x^{max} - C_x^{min}}{C_x^{max} + C_x^{min}}\right)^2}, \tag{25}$$

where ε_v—relative error of velocity evaluation; $\varepsilon_p = 5.0 \times 10^{-3}$—relative error of pressure measuring (0.5/100 = 0.005); $\varepsilon_T = 7.4 \times 10^{-3}$—relative error of temperature measuring (0.2/(300 − 273) = 0.0074); $\varepsilon_F = 2.0 \times 10^{-2}$—relative error of temperature measuring (2/100 = 0.02); $\varepsilon_D = 5.6 \times 10^{-3}$—relative error of diameter measuring (0.05 × 0.01/0.09 = 0.0056); and C_x^{min} = 1.1, C_x^{max} = 1.2—minimum and maximum values of the drag force coefficient, respectively.

According to Formula (25), ε_v = 0.045. Therefore, the relative error of velocity evaluation does not exceed 5%. Particularly, for the force F = 12.3 N, the evaluated outlet velocity (23) is in a range of v_{out} = 527–550 m/s. This value corresponds to the numerically obtained velocity, with a relative error that does not exceed 6.7%. A decrease in the actual velocity is due to additional frictional forces and reduced pressure after the outlet, which were not accounted for in the above model.

3.5. Rational Designs of Innovative Jet Nozzles

3.5.1. Spindle-Toroidal-Shaped Streamlined Body

First, it is proposed to replace the throat (with a diameter D_t) and outlet section of the traditional nozzle with a cylindrical outlet with initial expansion (from D_t to D_{out}) by applying an internal streamlined body (Figure 8).

The shape of the streamlined body (Figure 8a) can be obtained according to the developed methodology; however, due to the complexity of Equations (11) and (12), an

approximation by the circular arc with the unknown radius R is proposed. In this case, the maximum diameter of the streamlined body is obtained by Equation (15).

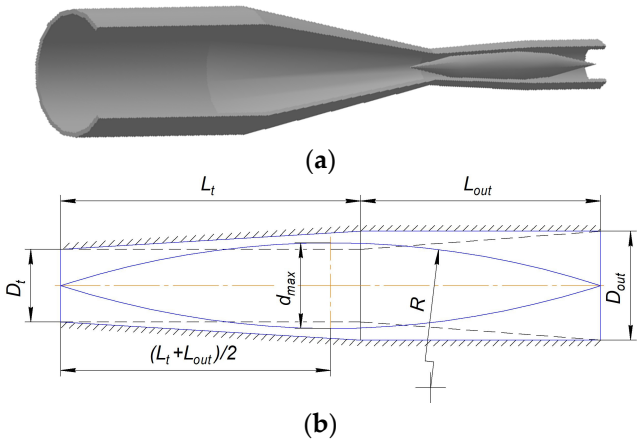

Figure 8. 3D model (**a**) and a throttle-to-outlet design (**b**) for a nozzle with spindle-toroidal-shaped streamlined body: black dotted line—the initial design; blue solid line—a new design with a streamlined body and a cylindrical outlet with initial expansion.

To evaluate the radius R, the following geometric dependence is applied according to the Pythagorean theorem:

$$\left(\frac{L_t + L_{out}}{2}\right)^2 + \left(R - \frac{d_{max}}{2}\right)^2 = R^2. \tag{26}$$

The only reliable solution to this equation allows evaluating radius R as follows:

$$R = \frac{1}{4}\left[d_{max} + \frac{(L_t + L_{out})^2}{d_{max}}\right]. \tag{27}$$

For the initial data presented in Table 2, the maximum diameter (15) of the streamlined body is d_{max} = 6.7 mm. Therefore, the radius (27) of this body is R = 77.1 mm.

Notably, by definition, the obtained streamlined body has a spindle-toroidal surface as a self-intersecting surface of revolution formed by rotating a circle around an axis that passes through the circle twice, and the following inequality is satisfied: $d_{max}/2 < R$.

Finally, the change in the streamlined body diameter is determined by the following equation:

$$d(x) = d_{max} - \left[R - \sqrt{R^2 - \left(x - \frac{L_t + L_{out}}{2}\right)^2}\right]. \tag{28}$$

The change in the nozzle's cross-sectional area is shown in Figure 9.

Because the spindle-toroidal surface approximates the streamlined body, a particular discrepancy arises. However, it also accelerates the air (up to 1.3 times) in the throttle section and extends the diffusor by up to 8.5%.

Nevertheless, despite this design's strengths, it has a disadvantage due to sharp edges at the throat entrance and the nozzle exit. This can potentially lead to undesirable formation of non-stationary Karman vortex tracks.

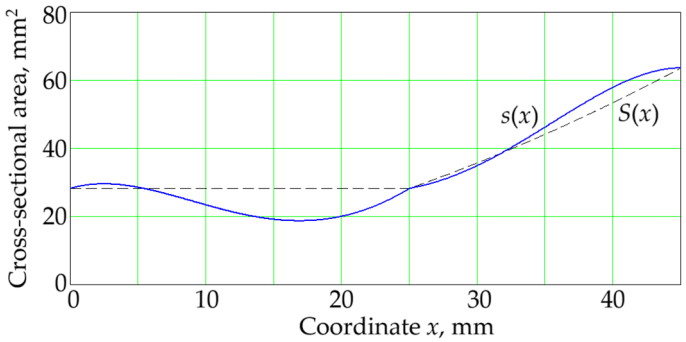

Figure 9. Changes in the cross-sectional areas: black dotted line—the initial nozzle design; blue solid line—the proposed nozzle design with spindle-toroidal-shaped streamlined body.

3.5.2. Ellipsoidal-Shaped Streamlined Body

To avoid the weaknesses of the above-mentioned nozzle design, it is proposed to replace the throat (with a diameter D_t) and the outlet section of the traditional nozzle with a single cylindrical section with an outlet diameter D_{out}, and to apply an internal streamlined body (Figure 10).

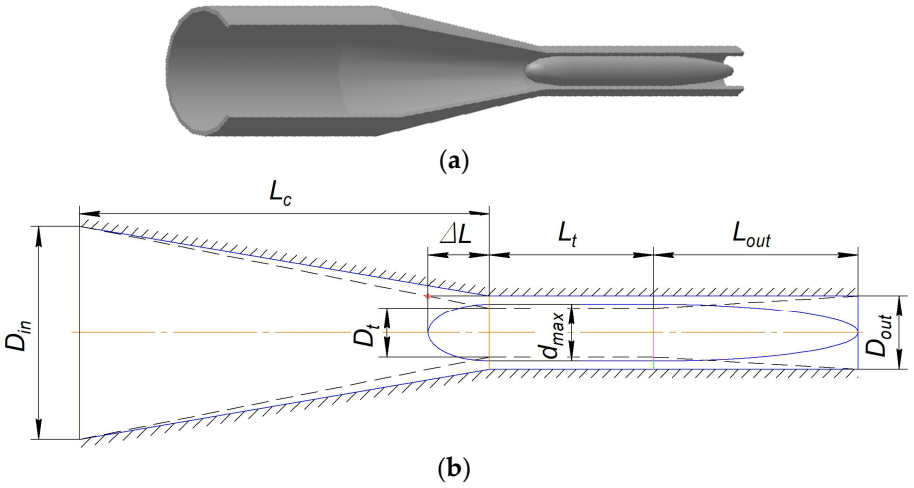

Figure 10. 3D model (**a**) and a throttle-to-outlet design (**b**) for a nozzle with ellipsoidal-shaped streamlined body: black dotted line—the initial design; blue solid line—a new design with a streamlined body and an extended cylindrical part.

The computational approach was developed to determine the nozzle geometry using the methodologies automatically (7)–(12). The program code, adapted from the PTC MathCAD v.14, is presented in Appendix A.

As a result of the calculations, the nozzle profile has been obtained as presented in Figure 11.

Like the previous design, this design features a streamlined body. However, its front and rear parts are not pointed, but smoothed. This avoids the disadvantage of the previous design, avoiding the formation of vortex tracks. Also, the middle part of the streamlined body is cylindrical. This allows annular flow to form in the nozzle's throttle and outlet sections.

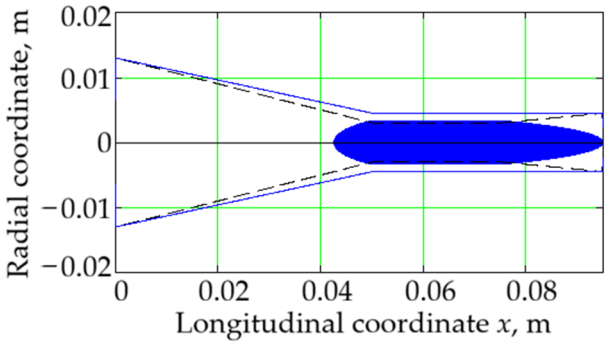

Figure 11. The automatically generated design scheme: black dotted line—the initial design; blue solid line—a new design; blue filled area—a streamlined body.

For smoother rounding of transitions and simplification of the manufacturing technology of the structure, it is proposed to form the front and rear parts of the streamlined body in the form of ellipsoids as surfaces of revolution with horizontal semi-axes ΔL (front part) and L_{out} (rear part), and also the vertical (radial) semi-axis $d_{max}/2$, equal to the radius of the cylindrical part. Notably, in this case, the value of d_{max} is also determined by Formula (15) and equals d_{max} = 6.7 mm, as in the previously proposed design.

To determine the semi-axis ΔL for the front part of the ellipsoidal body, the following geometric relationship is used (Figure 10a):

$$D_{in} - \frac{D_{in} - D_t}{L_c}(L_c - \Delta L) = D_{out}, \tag{29}$$

from which the following analytical dependence can be obtained:

$$\Delta L = \frac{D_{out} - D_t}{D_{in} - D_t} L_{in} = \frac{\beta_{out} - 1}{\beta_{in} - 1} L_c, \tag{30}$$

where $\beta_{in} = D_{in}/D_t$—a ratio of inlet-to-throat diameters.

For the initial data presented in Table 2, this ratio equals β_{in} = 4.33, and the semi-axis of the ellipsoid ΔL = 7.5 mm.

Radii of rounding for the front and rear parts are as follows, respectively:

$$r_{in} = \frac{d_{max}^2}{4\Delta L};\ r_{out} = \frac{d_{max}^2}{4L_{out}}. \tag{31}$$

These values are numerically equal to r_{in} = 1.5 mm and r_{out} = 0.5 mm, respectively.

Finally, the change in the streamlined body diameter is determined by the following dependencies:

$$d(x) = \begin{cases} d_{max}\sqrt{1 - \left(\frac{x - L_c}{\Delta L}\right)^2},\ L_c - \Delta L \le x < L_c; \\ d_{max},\ L_c \le x < L_c + L_t; \\ d_{max}\sqrt{1 - \left(\frac{x - L_c - L_t}{\Delta L}\right)^2},\ L_c + L_t \le x < L_c + L_t + L_{out}. \end{cases} \tag{32}$$

Because an ellipsoidal surface has approximated the streamlined body's shape, a certain discrepancy occurs (Figure 12), with a maximum value of 7.1%.

Notably, for the initial design presented in Table 2, for which ψ = 0.009/0.006 = 1.5, the Reynolds number is reduced by a factor of K = 2.6 in the last two developed models. This additionally proves the efficiency of the proposed nozzles.

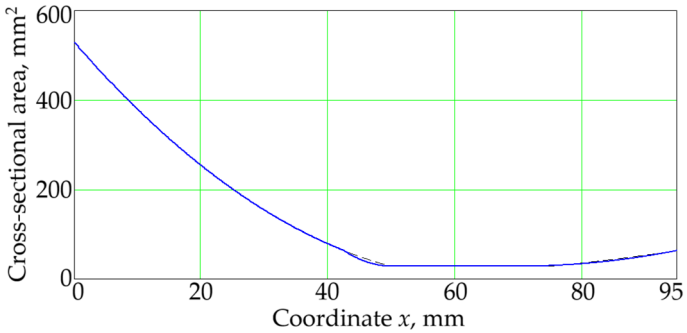

Figure 12. Changes in the cross-sectional areas: black dotted line—the initial nozzle design; blue solid line—the proposed nozzle design with ellipsoidal-shaped streamlined body.

3.6. CFD Modeling Results for Innovative Nozzles

3.6.1. Spindle-Toroidal-Shaped Streamlined Body

Numerical results of CFD modeling for the developed nozzle with a streamlined body of a spindle-toroidal shape are presented below. In particular, the axial pressure distribution (Figure 13) exhibits a monotonic decrease from the inlet stagnation region to the nozzle exit, consistent with the traditional model and compressible flow acceleration in a confuser–diffuser nozzle. As in the conventional model, velocity increases with the flow direction, with gradual acceleration in the converging section and a relatively rapid rise near the throat (Figure 14).

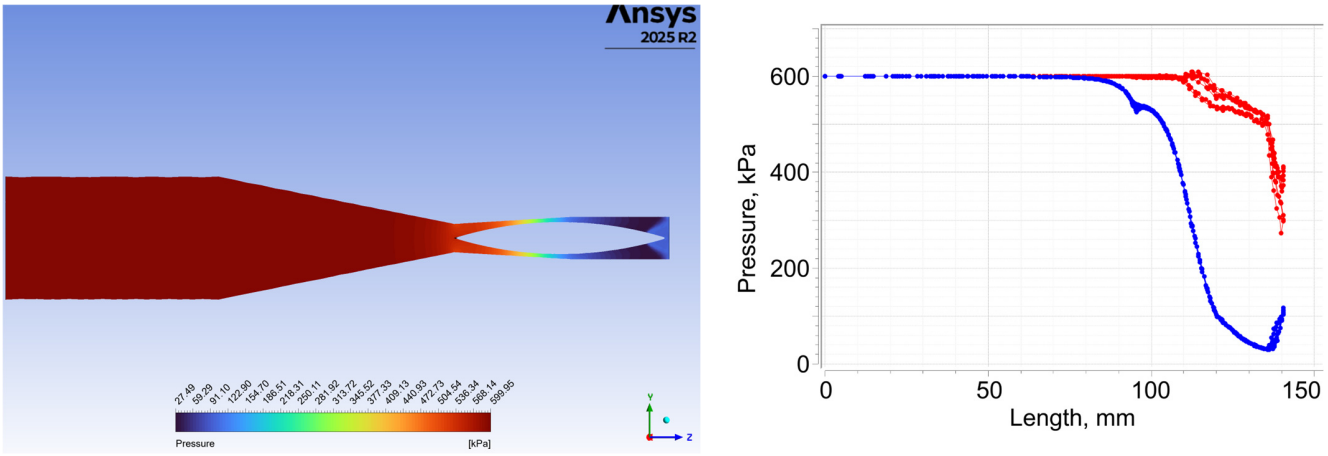

(**a**) (**b**)

Figure 13. Pressure distribution for a nozzle with the spindle-toroidal-shaped streamlined body: (**a**) contour plot; (**b**) graphs (red line—total pressure; blue line—static pressure).

Since the throat extends to the outlet, the velocity approaches sonic speed farther along, at the outlet's midpoint. Moreover, a local pressure change is suppressed to about 20 kPa, 3.0 times lower than for the traditional design. A slight downstream velocity gradient change is also suppressed.

Downstream of the outlet, the pressure continues to decrease as the cross-sectional area of the streamlined body decreases, indicating supersonic expansion. The maximum velocity, about v_{max} = 580 m/s, is reached near the outlet section, which is 3.0% higher than for the traditional nozzle.

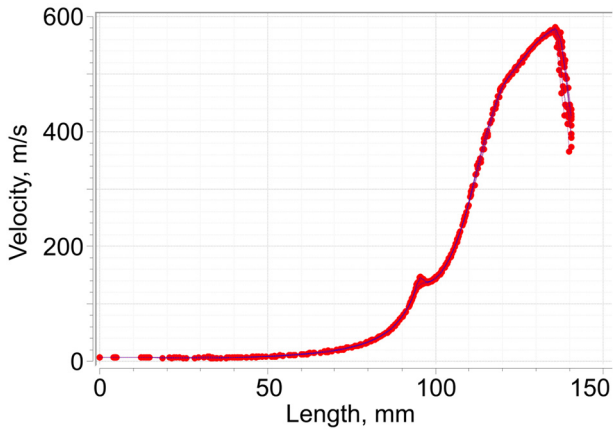

Figure 14. Velocity distribution graph for a nozzle with the spindle-toroidal-shaped streamlined body.

Also, due to the conversion of internal energy into kinetic energy, the static temperature decreases with increasing nozzle length (Figure 15). Like for the traditional nozzle, the temperature change is most significant in the region where the flow accelerates to supersonic speeds. A minor temperature rise (about 5 °C) also occurs.

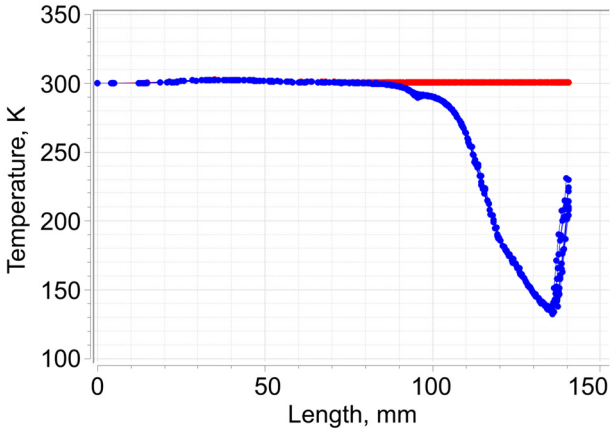

Figure 15. Temperature distribution graphs for a nozzle with the spindle-toroidal-shaped streamlined body (red line—total temperature; blue line—static temperature).

3.6.2. Ellipsoidal-Shaped Streamlined Body

Numerical results of CFD modeling for the developed nozzle with a streamlined body of an ellipsoidal shape are presented as follows. The axial pressure distribution (Figure 16) decreases from the inlet to the outlet, consistent with both the traditional model and the nozzle with a spindle-toroidal, streamlined body. As in the previous two models, the velocity increases with the flow direction (Figure 17). However, no rapid change in nozzle length is observed, indicating that local pressure drops are suppressed.

The maximum velocity, about v^{max} = 550 m/s, is reached near the outlet section, which is 3.0% lower than for the traditional nozzle.

Also, as in the previous two designs, the static temperature decreases with increasing nozzle length (Figure 18). However, no sudden temperature rise is observed.

Since the pressure profile does not have a local abrupt increase in the vicinity of the throat, a local pressure change is absent. The absence of such discontinuity also indicates a fully isentropic expansion mode. A smooth, monotonic increase in velocity also occurs.

Overall, the pressure, velocity, and temperature profiles confirm the operation of the nozzle with an ellipsoidal, streamlined body at a high-pressure ratio and validate the absence of local pressure changes.

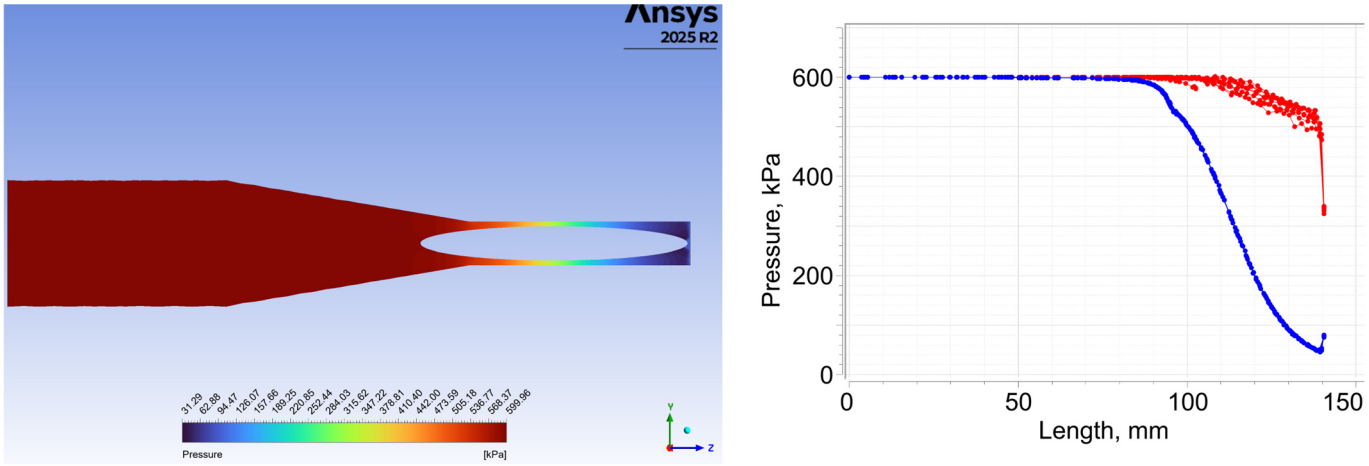

Figure 16. Pressure distribution for a nozzle with the ellipsoidal-shaped streamlined body: (**a**) contour plot; (**b**) graphs (red line—total pressure; blue line—static pressure).

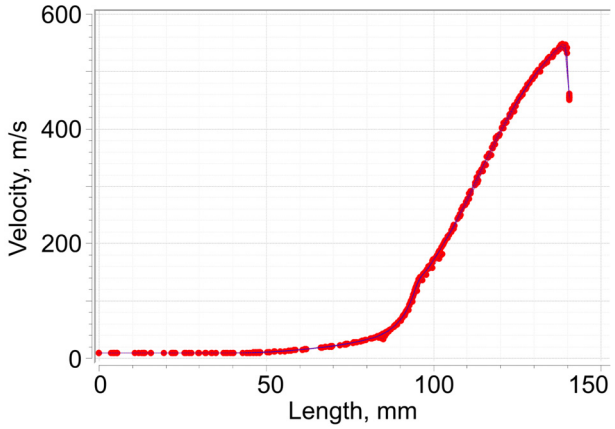

Figure 17. Velocity distribution graph for a nozzle with the ellipsoidal-shaped streamlined body.

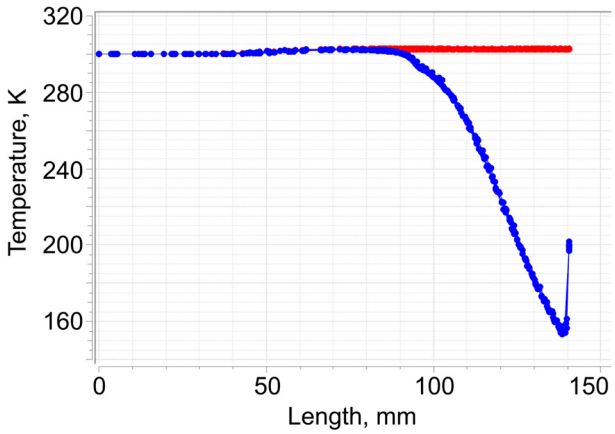

Figure 18. Temperature distribution graphs for a nozzle with the ellipsoidal-shaped streamlined body (red line—total temperature; blue line—static temperature).

3.7. A Prototype of an Innovative Nozzle

A summary of the comparative analysis of the proposed nozzle designs is presented in Table 5.

Table 5. A comparative analysis of the designed nozzles.

Static Pressure, kPa			Velocity, m/s (% *)			Static Temperature, K		
Inlet	Outlet	Local Pressure Change	Inlet	Outlet	Local Velocity Change	Inlet	Outlet	Local Temperature Change
Traditional design								
600	60–80	60	0	565	35	300	145	15
Nozzle with the spindle-toroidal-shaped streamlined body								
600	60–80	20	0	580 (+3.0%)	10	300	145	5
Nozzle with the ellipsoidal-shaped streamlined body								
600	40–80	0	0	550 (−3.0%)	0	300	150	0

* A change compared to the traditional design.

Thus, the introduction of a spindle-toroidal, streamlined body enabled the production of a nozzle with an increased outlet velocity and a significant reduction in the local pressure change.

Since the use of an ellipsoidal-shaped streamlined body, although it slightly reduces the outlet velocity, allows avoiding the negative effect (as shown in Figures 16b, 17 and 18), the related device has been chosen as a prototype. The corresponding assembly drawing is presented in Figure 19. Also, a summary of the expected characteristics of the developed prototype is presented in Table 6.

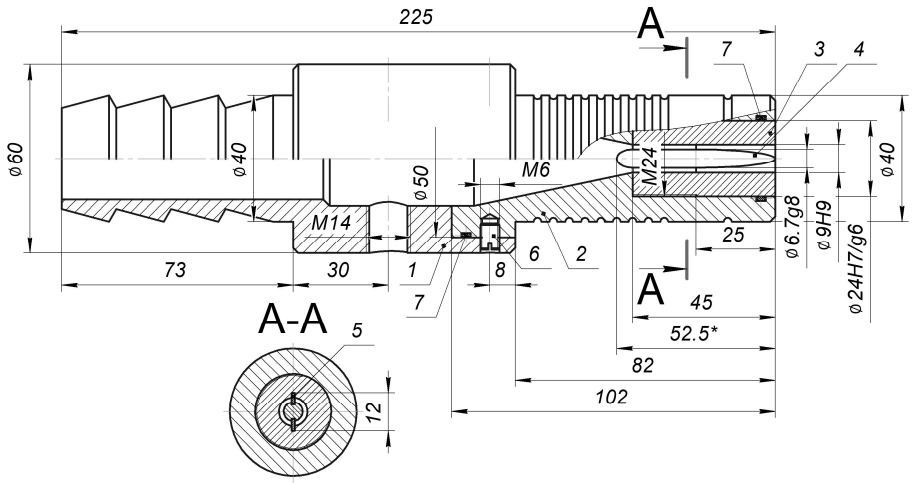

Figure 19. An assembly drawing of the prototype: 1—housing; 2—bushing; 3—insert; 4—streamlined body (* reference size); 5—pin; 6—screw; 7—sealing ring.

The transition from a cylindrical jet produced by a traditional nozzle to an annular jet in the proposed prototype with a streamlined body offers several significant technological and aerodynamic advantages.

First, the annular jet creates conditions for active entrainment and mixing of ambient air. As a result, the homogeneity of the temperature field and the phase composition of the mixture improves, creating the prerequisites for increased efficiency of heat and mass transfer.

Second, the annular jet leads to a uniform velocity distribution and, accordingly, reduces mechanical loads on the nozzle walls, thereby reducing erosion and local pressure change.

Third, the annular jet naturally creates an annular region, which helps reduce turbulent disturbances in the gas flow and stabilize it. The annular jet also improves heat transfer, contributing to a uniform distribution of the thermal load and reducing local temperature gradients, which are critically essential for the most loaded elements. The annular jet also helps prevent a local pressure change, significantly reducing the acoustic load and, accordingly, the noise and vibration levels of the whole installation.

Also, compared to traditional nozzles, it is assumed that the proposed prototype will prevent emergency boiler operation modes (especially during boiling) by enabling self-regulation of throughput (Figure 20).

Moreover, while addressing the problems of traditional nozzles, the proposed design could simultaneously improve the manufacturability of the main elements by incorporating a replaceable insert with a streamlined body.

Table 6. Expected characteristics of the developed prototype.

Characteristics	Traditional Nozzle	Developed Nozzle
Flow control	Not available	Possible (streamlined body)
Aerodynamic resistance	High (higher *Re* numbers)	Low (lower *Re* numbers)
Jet stabilization	Low (cylindrical flow)	High (annular flow)
Scalability	A new nozzle is required for each diameter	Adaptation to different cross-sections (streamlined body)
Energy efficiency	Unchangeable	Higher (lower hydraulic losses)
Material costs	High	Reserves by intensifying operating processes
Reliability in off-design and transient regimes	Limited (possible failure of other elements)	High (possibility to adjust the streamlined body position)

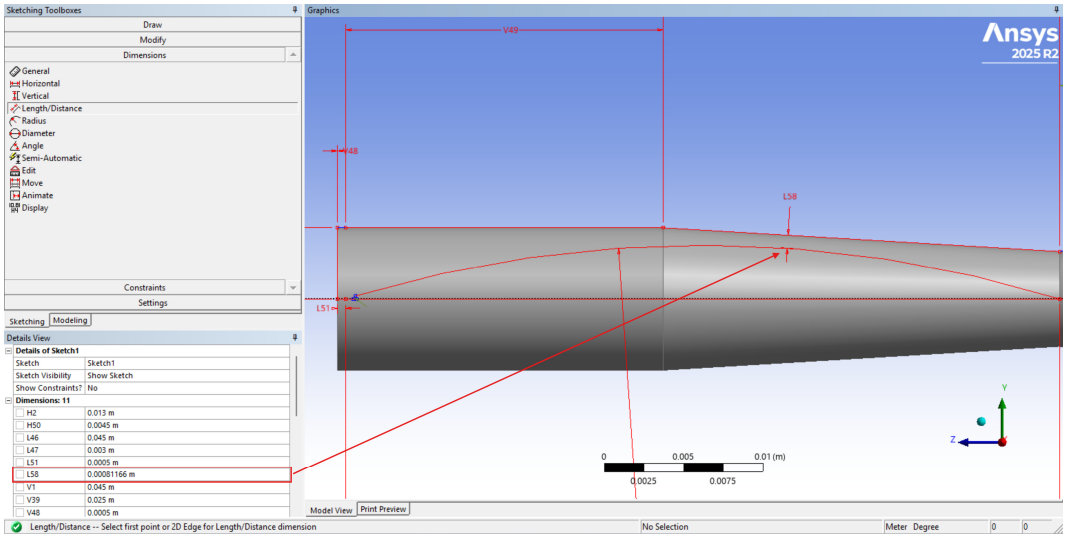

Figure 20. The possibility of self-regulation of throughput.

4. Conclusions

The article aims to improve the efficiency of nozzle devices by exploiting internal flow reserves through rational modifications to the working process in the flow passage. Based on analytical, numerical, and experimental investigations, it is demonstrated that controlling the internal flow structure with an internal streamlined body leads to a substantial improvement in gas-dynamic performance.

It has been established that the proposed nozzle designs provide a 3.0 times reduction in the pressure jump for the spindle-toroidal configuration and its complete elimination for the ellipsoidal configuration.

It has also been shown that the developed designs reduce the Reynolds number by up to 2.6 times in the throat region, resulting in lower turbulence intensity.

Moreover, the spindle-toroidal design shows an approximately 3.0% increase in the maximum outlet velocity, while the ellipsoidal configuration ensures smoother expansion and a more uniform velocity profile.

Experimental measurements of jet thrust confirm the CFD predictions with a deviation of 2.6–6.7%, while the numerical error in predicting total velocity and total temperature does not exceed 5.8% and 4.7%, respectively.

It is shown that axial displacement of the internal streamlined body enables targeted control of the flow rate and energy characteristics of the nozzle without altering the cross-sectional area distribution $S(x)$.

Further research will focus on extended studies of friction, erosion, service life, and energy efficiency indicators of the developed nozzles, as well as on extending adaptive control capabilities by optimizing the position, geometry, and kinematics of the streamlined body and additional flow-stabilizing elements, while considering shock waves and vortex shedding. Additional design features, such as the insert's rotational capability and spiral grooves, will create further opportunities to influence the flow structure and the pressure and velocity fields along the channel.

Author Contributions: Conceptualization, I.P.; methodology, I.P. and V.B.; software, M.O., M.M. and O.C.; validation, V.B.; formal analysis, M.O. and M.M.; investigation, I.P., V.B., M.O. and O.C.; resources, V.B.; data curation, O.C.; writing—original draft preparation, I.P. and V.B.; writing—review and editing, M.O. and O.C.; visualization, I.P. and O.C.; supervision, I.P.; project administration, V.B.; funding acquisition, M.O. All authors have read and agreed to the published version of the manuscript.

Funding: This research was funded by the Ministry of Education and Science of Ukraine, R&D project "Development of a mobile ejector-cleaning unit for the restoration of buildings, structures and equipment after fires in the war period", grant number 0124U000636. This research was also funded by the Ministry of Education and Science of Poland, SBAD project.

Data Availability Statement: The original contributions presented in this study are included in the article. Further inquiries can be directed to the corresponding author.

Conflicts of Interest: The authors declare no conflicts of interest.

Appendix A

Table A1 presents the initial data for the nozzle design.

Table A1. A matrix *DL* of the geometrical parameters (diameters *D* and lengths *L*, m).

Section	Diameter *D*, m	Length *L*, m
Section 1	0.026	0.050
Section 2	0.006	0.025
Section 3	0.006	0.020
Section 4	0.009	0 *

* A final zero-length section is needed to complete the design scheme by the outlet diameter D_{out}.

The initial index of the array: $ORIGIN := 1$.

The throttle diameter, mm: $D_t = 9$.

The total number of rows: $n := rows(DL)$.

Column-vectors of diameters and lengths, respectively: $D := DL^{<1>}$; $L := DL^{<2>}$.
A cycle for cylindrical and conical shapes formation: $i := 1, 2, \ldots, n-1$;

$$(ab_i)_{1,1} := 1;\ (ab_i)_{1,2} := 0,\ \text{if } i \equiv 0;\ (ab_i)_{1,2} := \sum_{k=1}^{i-1} L_k,\ \text{if } i > 0;$$

$$(ab_i)_{2,1} := 1;\ (ab_i)_{2,2} := \sum_{k=1}^{i} L_k;\ a_i := (ab_i)_1;\ b_i := (ab_i)_2.$$

Formation of an initial nozzle profile using step function $\Phi(\cdot)$:

$$d_0(x,i) := (a_i + b_i \times x) \times \Phi(x) \times (1 - \Phi(x - \sum_{k=1}^{i} L_k)),\ \text{if } i \equiv 0;$$

$$d_0(x,i) := (a_i + b_i \times x) \times \Phi(x - \sum_{k=1}^{i-1} L_k) \times (1 - \Phi(x - \sum_{k=1}^{i} L_k)),\ \text{if } i > 0; d_0(x) := \sum_{i=1}^{n-1} d_0(x,i).$$

Formation of a new nozzle profile:

$$d_1(x,i) := ({D_t}^2 - (a_i + b_i \times x)^2)^{0.5} \times \Phi(x) \times (1 - \Phi(x - \sum_{k=1}^{i} L_k)),\ \text{if } i \equiv 0;$$

$$d_1(x,i) := ({D_t}^2 - (a_i + b_i \times x)^2)^{0.5} \times \Phi(x - \sum_{k=1}^{i-1} L_k) \times (1 - \Phi(x - \sum_{k=1}^{i} L_k)),\ \text{if } i > 0;$$

$$d_1(x) := \sum_{i=1}^{n-1} d_1(x,i).$$

Change in the cross-sectional area for the initial and the new nozzles:

$$S_0(x) := \pi {d_0(x)}^2/4;\ S_0(x) := \pi({D_t}^2 - {d_1(x)}^2)/4.$$

References

1. Prevost, T.; Battaglioli, S.; Jenkins, R.; Robinson, A.J. Enhancing jet array heat transfer: Review of geometric features of nozzle and target plates. *Int. J. Thermofluids* **2022**, *16*, 100203. [CrossRef]
2. Zhao, D.; Zhang, Y.; He, Q.; Sun, C.; Bi, M. Hydrodynamic and flow field characteristics of water jet propulsion under mooring conditions. *J. Mar. Sci. Eng.* **2022**, *10*, 953. [CrossRef]
3. Wu, Z.; Wang, H.; Guo, H.; Gu, M.; Jiang, J.; Chen, S.; Huang, J.; Fan, S. Experimental investigation and application of mine airflow purification and reuse technology. *Environ. Technol. Innov.* **2021**, *24*, 102035. [CrossRef]
4. Shen, S.-L.; Njock, P.G.A.; Zhou, A. Influence of nozzle structure on effectiveness of jet grouting operations and its optimal design. *Geoenergy Sci. Eng.* **2023**, *226*, 211788. [CrossRef]
5. Teja, K.M.V.R.; Prasad, P.I.; Reddy, K.V.K.; Banapurmath, N.R.; Soudagar, M.E.M.; Khan, T.M.Y.; Badruddin, I.A. Influence of combustion chamber shapes and nozzle geometry on performance, emission, and combustion characteristics of CRDI engine powered with biodiesel blends. *Sustainability* **2021**, *13*, 9613. [CrossRef]
6. Khaled, M. Enhancing thermal performance of water-air cross flow heat exchangers through upstream nozzle design and unit division. *Int. J. Thermofluids* **2025**, *27*, 101223. [CrossRef]
7. Yang, B.; Chen, J.; Li, J.; Xie, W.; Wu, Q.; You, D.; Huang, S.; Sun, S.; Jiang, Z. A numerical study on the design of a diffuser nozzle for pulsed-jet cleaning of cone filter cartridges. *Atmosphere* **2025**, *16*, 379. [CrossRef]
8. Zhang, G.; Wang, X.; Chen, J.; Tang, S.; Smołka, K.; Majkut, M.; Jin, Z.; Dykas, S. Supersonic nozzle performance prediction considering the homogeneous-heterogeneous coupling spontaneous non-equilibrium condensation. *Energy* **2023**, *284*, 129274. [CrossRef]
9. Blanco, D.; Muñoz-Cobo, J.L.; Berna, C. Experimental analysis of jet expansion geometry and the influence of pressure waves on the behavior of air discharge processes in subcooled stagnant water. *Nucl. Eng. Technol.* **2025**, *57*, 103768. [CrossRef]

10. Singh, J.; Zerpa, L.E.; Partington, B.; Gamboa, J. Effect of nozzle geometry on critical-subcritical flow transitions. *Heliyon* **2019**, *5*, e01273. [CrossRef]
11. Chen, X.; Pan, H.; Chen, L. Effect of nozzle geometry on erosion characteristics in abrasive water jet: Experimental and numerical analysis. *Lubricants* **2025**, *13*, 132. [CrossRef]
12. Khan, H.; Lemma, T.A.; Soon, W.P.K.; Vijayakumaran, H.; Marode, R.V. A critical review on the comprehensive assessment of supersonic separator technologies for enhanced gas processing and CO_2 removal efficiency. *Results Eng.* **2025**, *28*, 106923. [CrossRef]
13. Zocca, M.; Gajoni, P.; Guardone, A. NIMOC: A design and analysis tool for supersonic nozzles under non-ideal compressible flow conditions. *J. Comput. Appl. Math.* **2023**, *429*, 115210. [CrossRef]
14. Wu, Z.; Hu, C.; Leng, P.; Zhao, W.; Deng, J.; Li, K.; Li, L. Effect of nozzle geometry features on the nozzle internal flow and cavitation characteristics based on X-ray dynamic imaging. *Nucl. Instrum. Methods Phys. Res. Sect. A Accel. Spectrometers Detect. Assoc. Equip.* **2024**, *1058*, 168831. [CrossRef]
15. Dai, L.; Haddad, A. Application of the method of characteristics to supersonic nozzle design and its comparison with CFD analysis. *Int. J. Adv. Nat. Sci. Eng. Res.* **2024**, *8*, 266–272.
16. Charrière, B.; Decaix, J.; Goncalvès, E. A comparative study of cavitation models in a Venturi flow. *Eur. J. Mech.—B/Fluids* **2015**, *49*, 287–297. [CrossRef]
17. De la Cruz-Ávila, M.; De León-Ruiz, J.E.; Carvajal-Mariscal, I.; Klapp, J. CFD turbulence models assessment for the cavitation phenomenon in a rectangular profile Venturi tube. *Fluids* **2024**, *9*, 71. [CrossRef]
18. Shi, F.; Zhao, J.; Dai, X.; Zhang, G.; Lu, Y.; Shang, Y. Structural optimization of nozzles for gas-liquid two-phase jets. *Fluid Dyn. Mater. Process.* **2025**, *21*, 2963–2980. [CrossRef]
19. Atmaca, M.; Çetin, B.; Ezgi, C.; Kosa, E. CFD analysis of jet flows ejected from different nozzles. *Int. J. Low-Carbon Technol.* **2021**, *16*, 940–945. [CrossRef]
20. Rao, S.M.V.; Jagadeesh, G. Novel supersonic nozzles for mixing enhancement in supersonic ejectors. *Appl. Therm. Eng.* **2014**, *71*, 62–71. [CrossRef]
21. West, L.G.M.; Simões, A.J.R.; Teixeira, L.d.R.; dos Anjos, I.S.M.; Devesa, A.S.B.d.F.; Oliveira, L.R.; Gomes, J.G.d.C.; Gomes, L.R.T.C.; Pereira, L.G.; Soares, L.C.S., Jr.; et al. Experimental and numerical analysis of nozzle-induced cavitating jets: Optical instrumentation, pressure fluctuations and anisotropic turbulence modeling. *Fluids* **2025**, *10*, 223. [CrossRef]
22. Shuja, S.Z.; Yilbas, B.S.; Khan, S.A. Flow emerging from annular-conical nozzle combinations and impinging onto a cylindrical cavity. *Int. J. Therm. Sci.* **2009**, *48*, 975–984. [CrossRef]
23. Narimani, Y.; Joulaei, A.; Shirvani, A.; Nili-Ahmadabadi, M.; Ha, M.Y. Shape optimization of annular transonic thrust nozzles via genetic algorithm and adjoint method. *Results Eng.* **2024**, *22*, 102255. [CrossRef]
24. Rukosuyev, M.; Baqar, S.; Nam, J.; Yun, H.; Jun, M.B.-G. Flame-assisted spray pyrolysis using an annular flame nozzle with decoupled velocity control. *J. Manuf. Mater. Process.* **2018**, *2*, 75. [CrossRef]
25. Wang, G.; Zou, J.; Chen, L.; Guan, B. Parametric study on configuration geometry effect on thrust performance of annular ED nozzles. *Propuls. Energy* **2025**, *1*, 2. [CrossRef]
26. Shuja, S.Z.; Yilbas, B.S.; Budair, M.O. Influence of conical and annular nozzle geometric configurations on flow and heat transfer characteristics due to flow impingement onto a flat plate. *Numer. Heat Transf. Part A Appl.* **2005**, *48*, 917–939. [CrossRef]
27. Park, K.A.; Choi, Y.M.; Choi, H.M.; Cha, T.S.; Yoon, B.H. The evaluation of critical pressure ratios of sonic nozzles at low Reynolds numbers. *Flow Meas. Instrum.* **2001**, *12*, 37–41. [CrossRef]
28. Sharapov, S.O.; Krmela, J.; Husiev, D.M.; Verbytskiy, A.R.; Bocko, J. Heat utilization in boiler plants by using liquid-vapor jet apparatus. *J. Eng. Sci.* **2024**, *11*, G1–G8. [CrossRef]
29. Meleychuk, O.; Vaneev, S.; Koroliov, S.; Miroshnichenko, O.; Pavlenko, I.; Ochowiak, M.; Włodarczak, S.; Krupińska, A.; Kruszelnicka, I. CFD analysis of steam jet-reactive turbines for sustainable energy: The critical role of boundary conditions. *J. Eng. Sci.* **2025**, *12*, F22–F31. [CrossRef]
30. Matsuo, S.; Kanesaki, K.; Nagao, J.; Khan, T.I.; Setoguchi, T.; Kim, H.D. Effects of supersonic nozzle geometry on characteristics of shock wave structure. *Open J. Fluid Dyn.* **2012**, *2*, 181–186. [CrossRef]
31. Song, J.; Chen, C.; Guo, Z.; Geng, M.; Rong, Z.; Wang, T.; Wang, J.; E, D.; Fan, J.; Sun, Y. Analysis of flow field, temperature, and inclusion evolution in a 12-strand tundish during ladle changeover process. *Metall. Mater. Trans. B* **2025**, *56*, 2700–2714. [CrossRef]
32. *ISO 1219-1:2012*; Graphical Symbols and Circuit Diagrams. International Organization for Standardization: Vernier, Switzerland, 2012.
33. *ISO 14617-1:2025*; Graphical Symbols for Diagrams. Part 1: General Rules. International Organization for Standardization: Vernier, Switzerland, 2025.
34. *EN 45501:2015*; Metrological Aspects of Non-Automatic Weighing Instruments. European Standard; European Standards Organizations: Brussels, Belgium, 2015.

35. Zhang, D.; Yuan, X.; Liu, S.; Zhu, K.; Liu, W. Experimental study of wall temperature effect on shock wave/turbulent boundary layer interaction in hypersonic aircraft. *Energy* **2023**, *263*, 125753. [CrossRef]
36. Hasegawa, M.; Chen, Y.-C.; Sakaue, H. Drag reduction study of a microfiber-coated cylinder. *Sci. Rep.* **2022**, *12*, 15022. [CrossRef] [PubMed]
37. Kline, S.J.; McClintock, F.A. Describing uncertain ties in single-sample experiments. *Mech. Eng.* **1953**, *75*, 3–8.

Disclaimer/Publisher's Note: The statements, opinions and data contained in all publications are solely those of the individual author(s) and contributor(s) and not of MDPI and/or the editor(s). MDPI and/or the editor(s) disclaim responsibility for any injury to people or property resulting from any ideas, methods, instructions or products referred to in the content.